The Astrophysical Journal, 639:969–974, 2006 March 10

ADAPTIVE-OPTICS-ASSISTED NEAR-INFRARED SPECTROSCOPY OF SVS 13 AND ITS JET[1]

C. J. Davis
Joint Astronomy Centre, 660 North A'ohoku Place, Hilo, HI 96720; c.davis@jach.hawaii.edu

B. Nisini
INAF—Osservatorio Astronomico di Roma, via di Frascati 33, 00040 Monteporzio Catone, Italy

M. Takami and T.-S. Pyo
Subaru Telescope, 650 North A'ohoku Place, Hilo, HI 96720

M. D. Smith
Armagh Observatory, College Hill, Armagh, Northern Ireland, UK

E. Whelan and T. P. Ray
Dublin Institute Advanced Studies, 5 Merrion Square, Dublin 2, Ireland

and

A. Chrysostomou
Centre for Astrophysics Research, University of Hertfordshire, Hatfield, Herts AL10 9AB, UK
Received 2005 August 30; accepted 2005 November 11

ABSTRACT

We present long-slit *H*- and *K*-band spectroscopy of the low-mass outflow source SVS 13, obtained with the adaptive-optics-assisted imager-spectrometer NACO on the VLT. With a spatial resolution of $<0\farcs25$ and a pixel scale of $0\farcs027$, we precisely establish the relative offsets of H_2, [Fe II], CO, H I, and Na I components from the source continuum. The H_2 and [Fe II] peaks are clearly associated with the jet, while the CO, H I, and Na I peaks are spatially unresolved and coincident with the source, as is expected for emission associated with accretion processes. The H_2 profile along the slit is resolved into multiple components, which increase in size, although they decrease in intensity, with distance from the source. This trend might be consistent with thermal expansion of packets of gas ejected during periods of increased accretion activity. Indeed, for the brightest component nearest the source, proper-motion measurements indicate a tangential velocity of $0\farcs028$ yr^{-1}. It therefore seems unlikely that this emission peak is associated with a stationary zone of warm gas at the base of the jet. However, the same cannot be said for the [Fe II] peak, for which we see no evidence for motion downwind, even though radial velocity measurements indicate that the emission is associated with higher jet velocities. We postulate that the [Fe II] could be associated with a collimation shock at the base of the jet.

Subject headings: ISM: Herbig-Haro objects — ISM: jets and outflows — stars: individual (SVS 13) — stars: pre–main-sequence

1. INTRODUCTION

With high spectral resolution observations one can probe emission-line regions at the bases of jets and thereby hope to distinguish between—or at least constrain—models of jet collimation and acceleration. Indeed, there are a number of diagnostic atomic and molecular lines in the near-infrared (near-IR) that are particularly useful for studying the more deeply embedded young stellar objects (YSOs; Davis et al. 2001, 2003; Pyo et al. 2002; Whelan et al. 2004; Takami et al. 2005; Nisini et al. 2005). Most notable are the [Fe II] and H_2 lines, which are found to be bright at the base of a number of jets from Class I protostars. The emission is usually blueshifted, the [Fe II] tracing a higher velocity component than the H_2, and offset along the axis of the jet by a few tens of astronomical units. These two species trace very different flow components: the [Fe II] derives from hot, dense, partially ionized gas ($T \sim 10,000$ K), while the H_2 traces low-excitation, shocked (or possibly fluoresced) molecular gas ($T \sim 2000$ K). These forbidden emission-line (FEL) and molecular hydrogen emission-line (MHEL) regions exist within a few hundred astronomical units of each outflow source and are therefore either within or very close to the primary jet collimation and acceleration zone. The H_2 may be entrained along the walls of the [Fe II] jet, or it may trace a cooler molecular disk wind ejected at larger disk radii.

As a further step toward a better understanding of these emission-line regions, here we present adaptive-optics (AO)–corrected *H*- and *K*-band spectra of the MHEL and FEL regions associated with SVS 13, the driving source of the HH 7-11 Herbig-Haro (HH) jet and molecular outflow (Chrysostomou et al. 2000; Bachiller et al. 2000). The source is located in the L1450 molecular cloud near the active low-mass star-forming region NGC 1333 in Perseus. SVS 13 is assumed to be at a distance of 300 pc (Cernis 1990; de Zeeuw et al. 1999); modeling of the HH bow shocks in the flow implies an inclination angle of $\sim 30^\circ$–50° with respect to the plane of the sky (Hartigan et al. 1987; Smith et al. 2003). The VLT observations presented here complement the earlier UKIRT observations of Davis et al. (2001, 2003), which yielded important kinematic information, although they lacked spatial resolution, and the more recent Subaru Telescope

[1] Based on Observations collected at the European Southern Observatory, Paranal, Chile (ESO programs 074.C-0408).

observations of Takami et al. (2005), in which a thorough excitation analysis has been made.

2. OBSERVATIONS

The combination of NAOS and CONICA at the European Southern Observatory (ESO) Very Large Telescope (VLT) provides AO correction using an IR-bright guide star in conjunction with near-IR spectroscopy. In our case, the jet source itself, SVS 13 ($J \sim 11.6$, $K \sim 8.1$), was used as the AO reference star. The S27-3-SH and S27-3-SK modes used yield a wavelength coverage of 1.37–1.72 and 2.02–2.53 μm at a spectral resolution of $R \sim 1500$. The slit width was 0.″172, the pixel scale along the slit was 0.″0270 $\pm$ 0.″0002 (measured from the offsets of a bright star along the slit), and the slit length was 28″. The *H*- and *K*-band observations were conducted in service mode on 2005 January 13 and 17, respectively. With the slit aligned along the SVS 13 jet axis (position angle = 159° east of north), the telescope was nodded between the object and blank sky six times in each wave band. Two 150 s exposures were obtained at each position.

The individual spectral images were bad-pixel-masked and flat-fielded using observations of a halogen lamp. Sky exposures were subtracted from object frames before wavelength calibration using argon arc spectra. Starlink FIGARO routines were used to correct for distortion along the slit axis, so that the wavelength calibration was constant along the spatial axis (along columns). The continuum associated with SVS 13 was then registered along the slit axis before co-addition of the data. Individual sky-subtracted images were compared to the shifted and co-added data in each wave band to make sure that the spatial resolution had not been compromised by this shifting and averaging process. From Lorentzian fitting to profiles taken through the SVS 13 continuum at various wavelengths, the full width at half maximum (FWHM) was found to vary between 0.″24 and 0.″40 in H and between 0.″19 and 0.″35 in K; in the averaged data the FWHM was 0.″26 $\pm$ 0.″03 in H and 0.″23 $\pm$ 0.″02 in K.

The B5 V bright star HIP 30943 ($V = 8.0$) was observed as a telluric standard. However, the extracted *H*- and *K*-band spectra of this source contain deep H I bracket absorption lines. Model Vega spectra were therefore used to remove these lines. Briefly, via an iterative process similar to that described by Vacca et al. (2003), the model data were scaled, smoothed and shifted before division into the HIP 30943 spectra. Comparison of the corrected HIP 30943 spectra with theoretical atmospheric transmission spectra presented by Vacca et al. (2003) showed that this process worked very well; the small difference in spectral type between Vega (A0 V) and the standard (B5 V) had no noticeable effect on the H I fitting. The atmospheric absorption features remaining in the corrected HIP 30943 spectra were subsequently aligned with equivalent features in the *H*- and *K*-band SVS 13 data, before the HIP 30943 spectra were "grown" into spectral images and divided into the SVS 13 spectral images.

3. NEAR-IR SPECTROSCOPY

H- and *K*-band spectral images are shown in Figures 1, 2, and 3. To more clearly show the line-emission features, the SVS 13 continuum has been removed from each image, row by row, by fitting a second-order polynomial to wavelength regions free of line emission. However, residual shot noise associated with the bright continuum does remain in some parts of the data.

As is the case in other spectroscopic studies (Davis et al. 2001; Takami et al. 2005), extended emission is observed only in H_2. However, for the first time, faint H_2 emission is also observed in the SVS 13 counterjet (positive offsets in Fig. 3). The H I

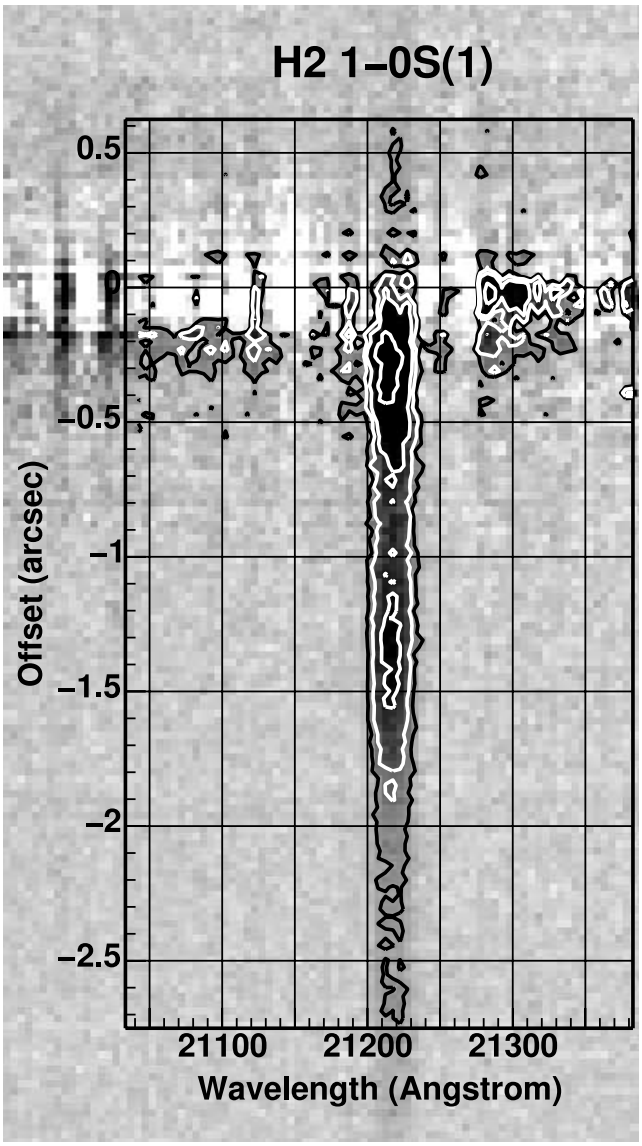

FIG. 1.—Contour plot extracted from the *K*-band spectral image showing the H_2 1–0 *S*(1) emission. Negative offsets are along the southeastern, blueshifted jet axis. The continuum associated with SVS 13 has been fitted and removed (see text).

Brackett lines in the *H* band and the CO, Brγ, and Na I lines in the *K* band all appear as compact peaks coincident with the continuum. The [Fe II] peak is also compact, although it is slightly offset along the blueshifted jet.

In Figure 4 we compare plots of the H_2 1–0 *S*(1) and [Fe II] 1.644 μm profiles traced along the slit, together with profiles of the adjacent continuum. The continuum plots are the average of profiles extracted slightly blueward and redward of the line in each case. The continuum profiles effectively show the spatial resolution of the observations, although they may be broadened slightly by nebulosity associated with SVS 13. Similar profile plots were produced for the CO 2–0 band head and Brγ line emission (not shown).

Only one component is evident in each of the CO, Brγ, and [Fe II] profiles, while as many as five separate peaks are identified in the H_2 profile (labeled in Fig. 4). From Lorentzian fitting, the offsets with respect to the source continuum position and the FWHM of the individual components seen in each line were measured. These are given in Table 1. The CO and Brγ peaks are unresolved and are precisely coincident, to within a few astronomical

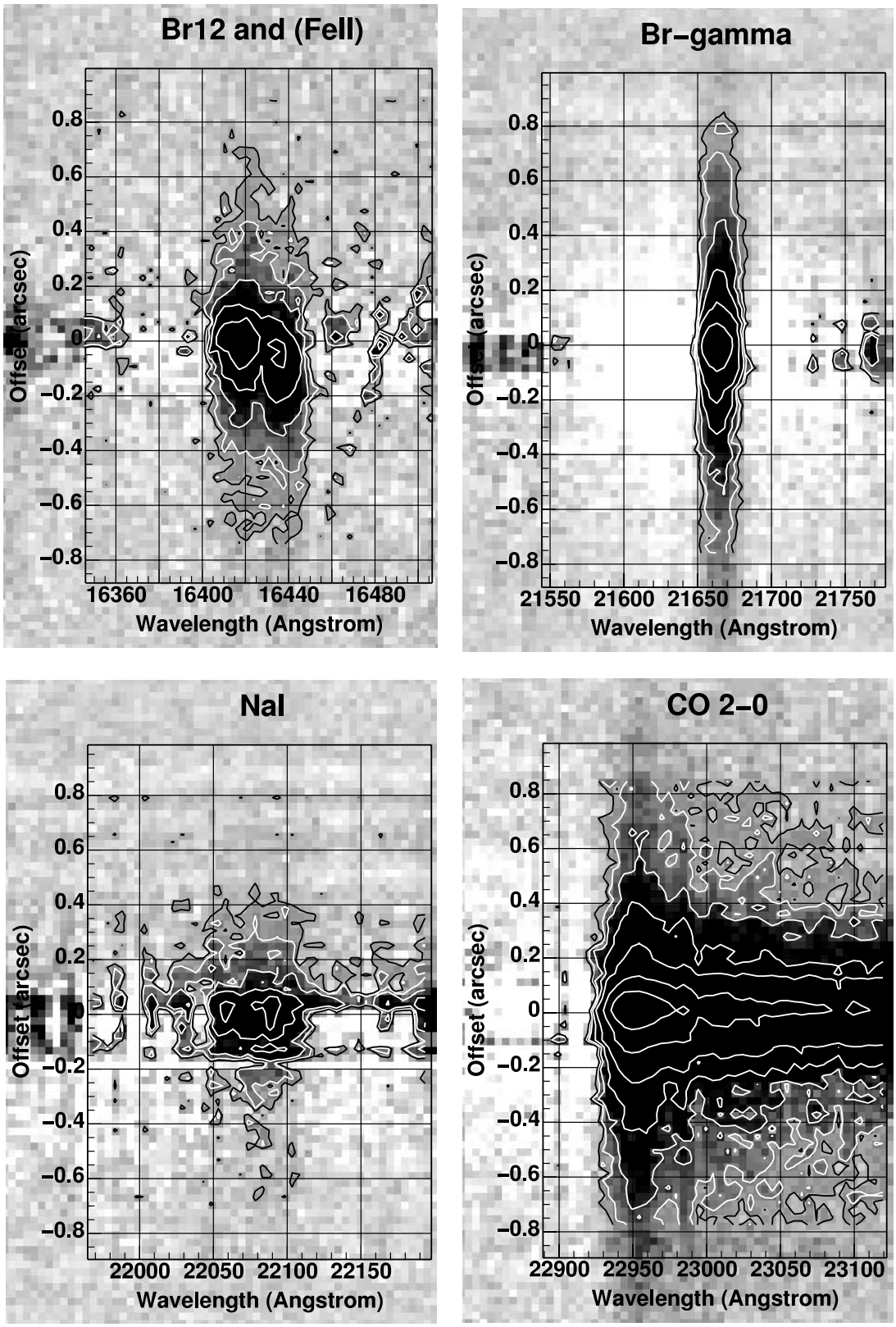

FIG. 2.—Contour plots extracted from the *H*- and *K*-band spectral images showing emission in select lines. The continuum has again been removed.

units, with the source continuum; we see no evidence for CO or H I components associated with the outflow.

The [Fe II] profile is, on the other hand, marginally resolved. In the echelle data of Davis et al. (2003) and Takami et al. (2005) a radial velocity of $\sim$140 km s^{-1} with respect to the systemic velocity was assigned to this component. Presumably this compact, high-velocity emission derives from a discrete knot or shock front near the base of the jet, rather than from an extended emission region.

In the H_2 data, we see an interesting trend in which the size (FWHM) of each component increases with distance from the

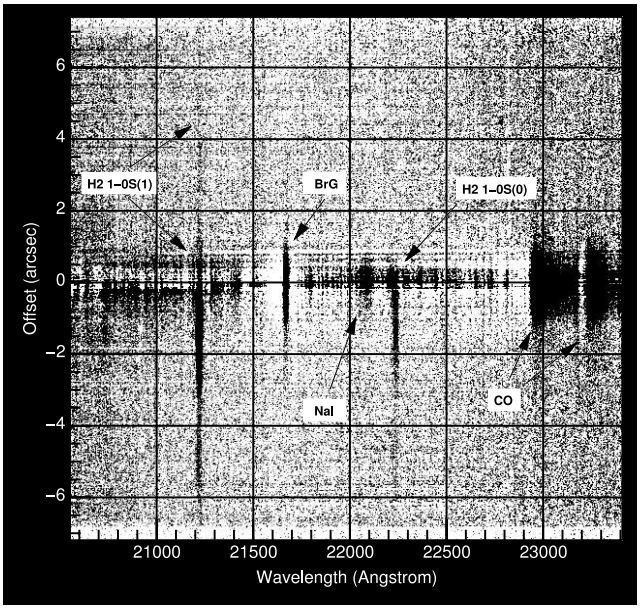

FIG. 3.—Continuum-subtracted *K*-band spectral image with a gray-scale stretch set to show the faint H_2 emission along the slit.

source (Table 1). Moreover, if the H_2 and [Fe II] trace the same jet material, this trend extends to the [Fe II] data; the closer a component is to the source continuum, the less extended it appears to be. The H_2 components also decrease in intensity with distance. This behavior could be explained by the cooling, decreased excitation, and expansion of "packets" of gas as they travel away from the source. A decrease in gas density and excitation temperature is inferred from the excitation analysis of Takami et al. (2005). A similar trend is also seen in small-scale jets from T Tauri stars (Bacciotti et al. 2000; Woitas et al. 2002).

Directly behind a fast-moving shock the very hot ($T \sim 10^3$–10^5 K) postshock gas will radiatively cool very rapidly, before the region has time to expand. However, the bulk of the material in the gas packet, *behind* the shock-front working surface, may expand adiabatically. If the pressure inside the warm ($T \sim 100$ K) gas packet approaches that of the surrounding medium as it expands, decreasing by a factor of ~10–100, and if at the same time the gas temperature in the packet decreases by a factor of 3–10 as it travels a distance of a few arcseconds (equivalent to the interknot spacing), then the packet might be expected to increase in volume by a factor of 1–30 or in diameter by a factor of 1–3. Isothermal expansion would result in greater expansion, while a lower pressure gradient would suppress expansion. Either way, the ratio is potentially consistent with the relative sizes of the H_2 components in Table 1.

TABLE 1
PARAMETERS FROM THE PROFILE FITTING

Line[a]	Offset (arcsec)	Offset (AU)	FWHM (arcsec)
H_2-1	0.29 ± 0.009	87.8 ± 3	0.44
H_2-2	1.19 ± 0.018	358 ± 6	1.3
H_2-3	2.0 ± 0.1	600 ± 30	1.5
H_2-4	4.8 ± 0.2	1428 ± 30	1.8
H_2-5[b]	0.28 ± 0.1	86 ± 30	1.0
[Fe II]	0.061 ± 0.004	18.3 ± 1.2	0.29
Brγ	0.001 ± 0.003	<0.9	0.19
CO	0.004 ± 0.003	<1.2	0.17

[a] Lorentzian fits to five components in H_2 (see Fig. 4); a single Lorentzian is fitted to the single peak in each of the extracted CO, [Fe II], and Brγ profiles.
[b] Possible component in the redshifted counterflow (positive offsets in Fig. 4).

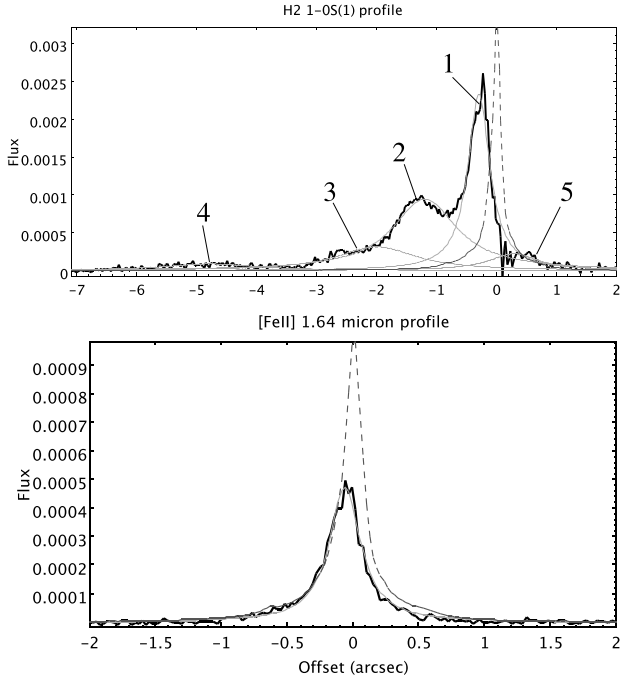

FIG. 4.—Profile plots showing the distribution of H_2 1–0 *S*(1) and [Fe II] 1.644 μm emission along the slit. The fine gray lines show Lorentzian fits to the data; one fit for the [Fe II] peak, but five fits to the H_2 data. The dashed line shows the profile through the continuum adjacent to each line.

4. PROPER MOTIONS

By comparing the VLT data with the earlier Subaru observations of Takami et al. (2005) we can measure, or at least set upper limits on, the proper motions (PMs) of the [Fe II] and H_2 components. The Subaru observations, although at higher spectral resolution ($R \sim 1.1 \times 10^4$), were not obtained with AO correction. However, the Subaru pixel scale (0.″060 ± 0.″002) does fully sample the seeing and the same slit position angle (159°) was used with both instruments. Offsets of emission features along the jet axis can therefore be measured accurately, and a direct comparison can be made between the VLT and Subaru observations (see Table 2). Note, however, that the Subaru slit was slightly wider than the VLT slit; 0.″30 versus 0.″172.

1. In the VLT *H*-band observations, the single [Fe II] component in Figure 4 may correspond to the high-velocity peak seen in the Subaru data, for which Takami et al. (2005) assign a radial velocity of ~140 km s^{-1}. Gaussian fitting yields an offset of 0.″10 ± 0.″01 for the Subaru peak. Curiously, the offset of the VLT peak in Table 2 implies that this feature has moved upwind, i.e., *closer* to the source. We certainly see no evidence for pronounced movement away from the jet source.

2. In the Subaru *K*-band echelle data two velocity components are resolved in H_2: a bright, low-velocity component (LVC) blueshifted by ~30 km s^{-1} that is spatially offset along the jet by 0.″23 ± 0.″01 and a fainter, more diffuse, high-velocity component (HVC) blueshifted by ~100 km s^{-1} that is offset by 1.″27 ± 0.″02. These two peaks, which are spatially as well as kinematically separate, probably correspond to the first two components in

TABLE 2
Component Offsets and Proper Motions

Line/Component [a]	VLT [b] Offset (arcsec)	Subaru [c] Offset (arcsec)	UKIRT [d] Offset (arcsec)	*HST* [e] Offset (arcsec)	PM [f] (arcsec yr^{-1})
H_2-1	0.29 ± 0.009	0.23 ± 0.01	...	...	0.028 ± 0.007
H_2-2	1.19 ± 0.018	1.27 ± 0.02	1.28 ± 0.01	∼1.1 ± 0.5[g]	<0.05
H_2-3	2.0 ± 0.1	...	2.13 ± 0.09	...	<0.03
H_2-4	4.8 ± 0.2	...	...	...	...
[Fe II]	0.061 ± 0.004	0.10 ± 0.01	...	...	−0.018 ± 0.006

[a] Lorentzian fits to five components in H_2 (see Fig. 4); a single Lorentzian is fitted to the single peak in each of the extracted CO, [Fe II], and Brγ profiles.
[b] VLT spectroscopy presented in this paper; data obtained on 2005 Jan 17.
[c] Subaru spectroscopy presented in Takami et al. (2005); data obtained on 2002 Nov 25.
[d] UKIRT Fabry-Pérot imaging from Davis et al. (2002); data obtained on 2000 Nov 23.
[e] *HST* NICMOS imaging from Noriega-Crespo et al. (2002); data obtained on 1998 Jan 9.
[f] PM measurements or upper limits; the negative value for the [Fe II] 1.644 μm peak reflects its apparent motion *toward* the source.
[g] Multiple components spread over an area of roughly 1″.

Figure 4. In Figure 5 we compare the Subaru data with smoothed VLT data: here the components clearly have a similar spatial offset, width, and brightness ratio. (Note that if the data were normalized to the HVC/component 2 peak, then the Subaru LVC would be brighter than the VLT component 1. Given the wider Subaru slit, one would expect this to be the case if the LVC traced a broader flow component than the HVC.) For the LVC/component 1, the offsets in Table 2 indicate a shift downwind of 0.″06 ± 0.″02 over the 783 day time interval between the Subaru and VLT observations. However, the HVC/component 2, like the high-velocity [Fe II] component, again exhibits no measurable PM away from the source.

Given the radial velocities of the HVC and LVC and assuming an inclination angle of 40° to the line of sight and a distance of 300 pc to SVS 13, then over the time period between the observations the H_2 LVC and HVC should have moved by 0.″04 (12 AU) and 0.″13 (38 AU) on the sky, respectively, while the [Fe II] feature should have moved by 0.″18 (53 AU). Clearly, only the H_2 LVC has a PM consistent with the observed radial velocity. Such consistency is expected if, for example, the gas is accelerated by a fast-moving shock front in a heavy jet.

The apparent lack of movement of the H_2 HVC could result from (1) the larger errors associated with the positional measurements of this fainter, more extended feature; (2) the blending of component 2 with component 3 (Table 1) in the lower spatial resolution Subaru data, so that the overall peak appears shifted downwind; or (3) the fact that the time interval between the observations is comparable to the molecular cooling time and therefore the timescale for morphological change, which could introduce unknown errors on the PM measurements.

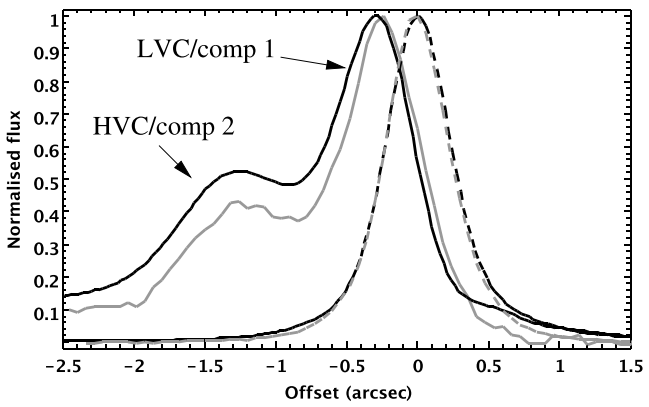

Fig. 5.—Comparison of the Subaru (*gray*) and VLT (*black*) H_2 profiles. The dashed lines show the adjacent continuum data. The VLT observations have been Gaussian-smoothed to the spatial resolution of the Subaru data.

The lack of a measurable PM in the [Fe II] peak is more difficult to explain. If the [Fe II] peak were associated with ejected clumps or bullets, then one would perhaps expect to see additional components along the flow axis (as is the case in H_2). Instead, the [Fe II] is confined to a single, very compact peak at the jet base. The [Fe II] could be associated with a stationary, collimating shock, similar to that described in the models of Ouyed & Pudritz (1994). If this is indeed the case, the collimation point would be at a distance of ∼20 AU from the source.

On the other hand, we may be observing two completely independent [Fe II] peaks in the Subaru and VLT data, rather than the same near-stationary feature. The Subaru feature may have faded, to be replaced by a new peak in the VLT observations. The cooling time, from 20,000 to 7000 K for dense (10^5–10^6 cm^{-3}), postshock gas will be of the order of weeks or even days (Smith 2003), so morphological changes are certainly possible. This might explain the apparent "upwind" movement of this feature.

A number of groups have attempted to *image* the emission-line region at the base of the SVS 13 outflow. Davis et al. (2002) used a Fabry-Pérot (FP) etalon to "boost" the line/continuum ratio in their data. The H_2 emission at the jet base is certainly evident in their image, although the poor spatial resolution of their observations (∼1″) somewhat limits their ability to extract spatial information. They do collapse their image along an axis perpendicular to the jet and attempt to subtract the continuum emission from the resulting profile (their Fig. 4). They identify a "peak" and a "plateau" along the jet axis, which may correspond to H_2 components 2 and 3 in the VLT data. We list the offsets of these features in Table 2.

Noriega-Crespo et al. (2002) used the *HST* to obtain high spatial resolution near-IR images of the HH 7-11 outflow. They present a continuum-subtracted H_2 image of SVS 13 (their Fig. 3). However, residual artifacts left over from the continuum subtraction, in the bright core but also in a ring of radius ∼1″, make identifying features within 0.″5–1.″0 of SVS 13 more or less impossible. However, they do detect and resolve the H_2 emission in the flow at offsets of >1″. Within 1″–2″ of SVS 13 the H_2 appears to comprise at least two knots superposed on a patch of moderately extended emission, suggesting a broad opening angle for the H_2 flow. Component 2 in the VLT data (the HVC in the Subaru

observations) may therefore constitutes *two knots*; we give a combined offset for these two features (measured along the VLT/Subaru slit axis) in Table 2 for reference.

Overall, the results from these two imaging surveys can only be used to confirm the presence of emission features. Uncertainties in the continuum subtraction limit their usefulness when measuring PMs. Notably, the compact LVC evident in both the Subaru and VLT spectroscopy was not extracted from the FP or *Hubble Space Telescope* (*HST*) images.

Clearly, follow-up observations with the NACO system are needed to better constrain the PM measurements discussed above, particularly for the [Fe II] peak and the H_2 components further downwind. Confirmation of the "stationary" [Fe II] peak would add credence to the collimation-shock interpretation. If we also ultimately find that the H_2 peaks do *not* move, then in H_2 we could be witnessing a warm, stationary region or perhaps a turbulent mixing layer between the jet and ambient medium at the jet base through which jet material flows, rather than discrete bullets or clumps ejected during episodes of increased accretion. However, given the tentative result for the LVC, and the fact that knots in Herbig-Haro jets and molecular flows typically do have large PMs (Reipurth & Bally 2001), for H_2 at least, this seems unlikely.

Finally, we mention that the dynamical age of the H_2 LVC/component 1 in the VLT data, when derived from its PM and offset in Table 1, is $\sim$10 yr. Notably, the optical outburst reported by Eislöffel et al. (1991) occurred roughly 15 yr before the observations reported here. Our results are thus reasonably consistent with the H_2 LVC being produced by this outburst and the associated increase in accretion.

REFERENCES

Bacciotti, F., Mundt, R., Ray, T. P., Eislöffel, J., Solf, J., & Camenzind, M. 2000, ApJ, 537, L49

Bachiller, R., Gueth, F., Guilloteau, S., Tafalla, M., & Dutrey, A. 2000, A&A, 362, L33

Cernis, K. 1990, Ap&SS, 166, 315

Chrysostomou, A., Hobson, J., Smith, M. D., Davis, C. J., & Berndsen, A. 2000, MNRAS, 314, 229

Davis, C. J., Ray, T. P., Desroches, L., & Aspin, C. 2001, MNRAS, 326, 524

Davis, C. J., Stern, L., Ray, T. P., & Chrysostomou, A. 2002, A&A, 382, 1021

Davis, C. J., Whelan, E., Ray, T. P., & Chrysostomou, A. 2003, A&A, 397, 693

de Zeeuw, P. T., Hoogerwerf, R., de Bruijine, J. H. J., Brown, A. G. A., & Blaauw, A. 1999, AJ, 117, 354

Eislöffel, J., Guenther, E., Hessman, F. V., Mundt, R., Poetzel, R., Carr, J. S., Beckwith, S. V., & Ray, T. P. 1991, ApJ, 383, L19

Hartigan, P., Raymond, J. C., & Hartmann, L. 1987, ApJ, 316, 323

Nisini, B., Bacciotti, F., Giannini, T., Massi, F., Eislöffel, J., Podio, L., & Ray, T. P. 2005, A&A, 441, 159

Noriega-Crespo, A., Cotera, A., Young, E., & Chen, H. 2002, ApJ, 580, 959

Ouyed, R., & Pudritz, R. E 1994, ApJ, 423, 753

Pyo, T.-S., Hayashi, M., Kobayashi, N., Terada, H., Goto, M., Yamashita, T., Tokunaga, A. T., & Itoh, Y. 2002, ApJ, 570, 724

Reipurth, B., & Bally, J. 2001, ARA&A, 39, 403

Smith, M. D. 2003, Ap&SS, 287, 195

Smith, M. D., Khanzadyan, T., & Davis, C. J. 2003, MNRAS, 339, 524

Takami, M., et al. 2005, ApJ, submitted

Vacca, W. D., Cushing, M. C., & Rayner, J. T. 2003, PASP, 115, 389

Whelan, E., Ray, T. P., & Davis, C. J. 2004, A&A, 417, 247

Woitas, J., Ray, T. P., Bacciotti, F., Davis, C. J., & Eislöffel, J. 2002, ApJ, 580, 336